Impact of Nonlinear Effects on a High-Frequency Seismic Landmine Detection System

Gregg D. Larson [a], James S. Martin[a], Peter H. Rogers[a],
Waymond R. Scott, Jr. [b], and George S. McCall II [c]
[a] School of Mechanical Engineering
[b] School of Electrical and Computer Engineering
[c] Georgia Tech Research Institute
Georgia Institute of Technology
Atlanta, GA 30332

ABSTRACT

A system is currently under development at Georgia Tech that uses both electromagnetic and elastic waves to detect and image buried landmines. The system generates elastic waves in soil using a surface-contacting transducer designed to preferentially excite Rayleigh waves, thus interrogating only the surface layers of the soil. These waves propagate through a region of interest and interact with buried landmines and clutter. Normal surface displacements are measured using a specially designed non-contact radar sensor that is scanned over the entire region. Both the speed with which this sensor can be scanned and the contrast between mines and background in the resulting images depend upon the signal-to-noise of the measurements made at each location. The level of the signal component in this ratio appears to be more sharply limited by nonlinear effects in the ground than by the capabilities of the elastic wave source that is currently being used in the system. A study was undertaken to characterize these effects in both the laboratory experimental model, in which the system was developed, and at a field test site. At both of these sites, strong nonlinearities were observed which limited the energy content of the interrogation signal. These may also degrade contrast in mine images by undermining linear assumptions in image processing algorithms thereby introducing artifacts that effectively enhance the noise.

Keywords: landmine, mine detection, nonlinearity, seismic waves

1. INTRODUCTION

Seismic/elastic techniques show considerable promise for the reliable detection of all types of buried mines, even low-metal anti-personnel mines. The reason for this is that mines have mechanical properties that are significantly different from soils and typical forms of clutter. For example, the shear wave velocity is approximately 20 times higher in the explosive and the plastics used in typical mines than in the surrounding soil [1]. In addition, mines are complex mechanical structures with a flexible case, a trigger assembly, air pockets, etc. This complex structure gives rise to structural resonances, nonlinear interactions, and other phenomenology that is atypical for both naturally occurring and man-made forms of clutter. Thus, this phenomenology can be used to distinguish a mine from clutter.

A system is under development at Georgia Tech that uses a radar-based displacement sensor for the local measurement of seismic displacements without physically contacting the soil surface [2, 3]. The non-contact nature of this sensor makes the system capable of interrogating the soil surface near or immediately above a buried mine. This substantially increases the measurable effects of the mine's presence over schemes which rely on elastic waves scattered by the mine to propagate to a remote sensor location [4]. Figure 1 depicts the present system configuration. The system consists of the non-contact sensor and the ground coupled seismic source. The source (an electrodynamic shaker resting on a narrow foot) excites an incident signal composed primarily of a

Rayleigh surface wave with measurable energy also propagating in other modes. Although this source design has not been optimized, experiments and limited numerical modeling suggest that a contact surface with a relative large frontal length (perpendicular to the propagation direction) and a relatively small total surface area preferentially excites Rayleigh waves, rather than bulk waves. Buried or partially buried sources were not considered since the ultimate goal of the research is to produce a system with both a scanning source and sensor. In system operation, the incident signal travels across the minefield and excites motion of soil near the surface that includes the buried mine(s). The sensor measures the surface normal component of this motion over an array of measurement locations. Sensor data are then processed in both space and time domains to yield an image of the minefield [5]. To interrogate the earth over the range of typical mine sizes and burial depths, the incident signal has a spectrum from 50 Hz to 1 kHz.

The imaging scheme that is employed in the current system achieves an acceptable signal-to-noise ratio (SNR) through linear pulse compression. The experimental data are acquired as transfer functions relating the measured surface displacements (with the radar sensor) to the input drive signal. While the current drive signal is a four second long frequency-modulated chirp that covers the frequency band of interest, other drive signals which span long time periods (typically several seconds) have been used. Multiplication of the transfer function by the desired pulse shape in the frequency domain and subsequent transformation of the result to the time domain provides the measured surface displacements as a function of time. The pulse compression scheme allows for improvement in SNR through either an increase in the level of the original drive signal or an increase in its duration. Increasing duration comes at the expense of slower data acquisition and therefore slower scanning. Increasing drive signal amplitude comes at the expense of nonlinearities that corrupt the linear assumptions of the pulse compression, thereby creating an artificial enhancement of the noise floor through compression artifacts. The present experimental study was motivated by the desire to determine an acceptable balance between SNR and drive signal characteristics for typical operating conditions.

The seismic mine detection system has been investigated experimentally over the past three years using a series of laboratory models of increasing size and complexity. Damp compacted sand was selected as the medium for these models because of the ease and repeatability it offered for the burial of mines, mine simulants, and clutter objects. Anecdotal evidence exists in the literature to suggest that this is a reasonable model for soils [6,7]. The published experimental data are sparse on the range of frequencies and depths that are of interest for this problem and are mostly limited to the characterization of soils within the linear regime. Scaling of published experimental data and theoretical results involving very different frequency ranges and material parameters requires a sufficient experimental database to justify the comparison, which does not presently exist. Additionally, results generated with the laboratory model suggest phenomena that may be linked to soil grain size or very near surface effects that thereby defy simple scaling.

The baseline sensors used in this study were ground-coupled accelerometers, as the radar-based displacement sensor is not currently configured for outdoor measurements. The accelerometers have the advantage of having comparable sensitivity to the radar sensor over most of the band of interest while being waterproof and robust in a comparatively hostile environment, functional in any orientation, and easily buried below the surface. They also offer a simple method for the construction of a physical array, whereas the radar sensor is currently a single sensor that is scanned to form a synthetic array. The synthetic array cannot easily distinguish between long-timescale changes, such as tidal motions of the water table, and short-timescale changes, such as dispersion of a propagating waveform. Unlike the laboratory environment, these factors cannot be controlled in the field. Single axis Vibra-Metrics VMI-9002A accelerometers, which were encapsulated in syntactic foam, and triaxial PCB W356-A12 accelerometers were used for these measurements. These both have 100 mV/g sensitivity and integral charge amplifiers. Data for all of the experiments were acquired simultaneously on up to 48 channels using a PC computer that housed three 12-bit resolution National Instruments analog-to-digital (A-to-D) data acquisition cards. Initial data, including all of the data from the field test site, were acquired without anti-aliasing filters. These were deemed unnecessary because the spectra of the interrogation signals were well characterized and previous experiments had demonstrated rapid attenuation of high frequencies with propagation distance in sand. Thus, it was assumed that moderate over-sampling of the data would be sufficient to

prevent aliasing effects. Unfortunately, although the Nyquist frequency was two octaves above the highest transmit frequency (1 kHz), and well above the dominant spectral components of the background noise, aliasing problems introduced by a wealth of harmonics in the system complicated the analysis of some of the data. Aside from this problem, the accelerometer system offered a SNR equivalent to that achieved by the radar sensor in the laboratory at 100 Hz. Since the radar sensor responded to displacement rather than acceleration, there was a 12 dB per octave SNR improvement associated with the accelerometers at high frequencies and a corresponding comparative degradation at low frequencies.

2. COMPARISON OF TEST SITES

Figure 2 shows the laboratory model and the field site. The laboratory model, which has been described in detail in a previous paper [2], is a 1.5 m deep wedge-shaped tank filled with 50 tons of masonry sand that is kept damp and compacted with a water table maintained 50 cm below the surface. The field test site is at the Navy beach adjoining the campus of the Naval Postgraduate School (NPS) in Monterey, California. This has been the site of ongoing micro-seismic experiments undertaken at NPS and is quite near a beach location extensively characterized by Bachrach, Nur, and Dvorkin in 1995 [8, 9]. Several different accelerometer array configurations were used at both sites. The cross configuration depicted in Figure 2 represents the largest of these. Tides varied the water level at the field site both during and between experiments. The dimensions shown are typical, although depth changes of up to 50 cm occurred during the experiments. This translated into horizontal changes of up to 10 m for the wave-washed region of the beach. Some of the experiments were performed at low tide on the harder sand below the high water mark. Others were performed at high tide on the softer dry sand above the high water mark. Similar propagation speeds were observed in both cases, although the wet sand results more closely matched those of the laboratory model. This is due to the similar water content of the sand near the surface and to the packing caused by wave action, which mimicked the artificial packing of the laboratory model. Figure 3 depicts waterfall plots generated by identical pulse compression of data taken at both the laboratory and field sites. The data shown here were reconstructed from transfer functions measured using a 4-second swept-frequency chirp covering the entire band of interest. The compressed drive signal was the first derivative of a Gaussian pulse centered at 400 Hz, which is typical of the drive signals that are used to image small mines. The plots in Figure 3 indicate the similarity between the laboratory model and field site. The data depicted were acquired with relatively low levels of excitation and therefore represent propagation in the linear regime at both sites. Two distinct arrivals are observed at each site. The first of these (any apparent earlier arrivals are caused by noise-induced processing artifacts) arrives with a group velocity of 170 m/s to 183 m/s, which is consistent with previously observed P-wave (compressional) velocities [8, 9] and with observations of leaky surface waves [10] at similar sites. Later investigations of this arrival in the laboratory model point out shortcomings with both of these earlier investigations, although the later interpretation appears to be the correct one. The series of small arrivals are probably reverberations of this first arrival. The second and largest pulse arrival propagates with a speed of 87 m/s to 90 m/s and is due to the Rayleigh surface wave. The peaks of this waveform have been clipped in the figure in order to display both wave types in a single graph. This speed is consistent with the other reported observations of Rayleigh waves in both sand and hard soil [7, 10]. The coda associated with the Rayleigh wave arrival is longer and more complex in the field data than in the laboratory because of the variety of surface and subsurface inhomogeneities at the field site. These include footprints, buried flotsam, and a water table that was inclined with respect to the ground surface and non-uniform due to wave action. Although identical pulse shapes were used with both data sets, there are also some differences in the shapes of the received signals: the data from the laboratory model have lower spectral content than the field data. This is due to a difference in the frequency response of the two different transducers that were used in these tests. A MB Electronics 20-lb. shaker was used as a source for the field tests, but this was damaged in shipping and replaced by a 100-lb. VTS shaker for the later laboratory measurements. Although the Rayleigh wave pulse has been clipped in these plots, dispersion is apparent in both the laboratory and field data. In a homogenous, isotropic, semi-infinite medium, these waves would be non-dispersive. The most likely cause for this dispersion is a vertical inhomogeneity in the sand. This

may be due to the depth dependence of water content (as hypothesized in [8, 9]) or to the lithostatic force on the lower strata (as in the earth's crust on large length scales [11]).

A second difference between the field site and the laboratory model is the horizontal anisotropy in the wave propagation introduced by the incline of the water table. Figure 4 shows a comparison of measurements made perpendicular to the direction of wave propagation for two cases from the field site: first, for a wave propagated along the shoreline, and second, for a wave propagated directly inland. The waveforms represent only the surface wave pulse (the faster arrivals are time-gated out) and are not clipped, but they have been normalized by their peak values to correct for the directivity of the source. The inland propagation measurement shows strong top/bottom symmetry along the array, as one would expect for an isotropic medium. The along-shore measurement, however, shows a distinctly different pulse shape arriving at the shoreward end of the array. This dispersion may be due to the narrowing dimension of waveguide between the surface and the water table or to a lowering of the wave speed with water content below complete saturation. This was observed by Bachrach, Nur, and Dvorkin [8, 9] for P-waves in a similar environment.

It is also interesting to note that a third difference between the laboratory model and the field site was in the observed ambient noise fields. This difference, surprisingly, favored the field site. In spite of wave action, wind, and foot traffic, the noise floors measured at the field site were entirely due to the instrumentation noise of the measurement system below 500 Hz. In contrast, the noise floor in the laboratory model has several distinctive features that can be attributed to artificial sources and couple into the model through the foundation of the building that houses it. On average, the laboratory measurements were made over a noise floor that was at least 4 to 6 dB higher than the field site's noise floor in the 50 Hz to 1 kHz band.

3. CHARACTERIZATION OF WAVE FIELDS

In homogenous media, two types of bulk wave propagation would be expected. These are the compressional wave (P-wave) and the shear wave (S-wave). The latter may be polarized orthogonally such that two independent shear waves may exist: the vertically and horizontally polarized shear waves (SV- and SH-waves). If the porosity of the medium is considered, then the P-waves may also be divided in into fast and slow Biot waves, which have been simultaneously observed in some soils [6]. The free surface of the sand permits the propagation of guided surface waves such as Rayleigh waves and leaky waves [12]. If inhomogeneities are considered, then other guided wave types may also be present at or near the surface. In order to determine which of these modes accounted for the arrivals observed in the data, an experiment was conducted with triaxial accelerometers installed in the laboratory experimental model. These were installed as both a linear array of accelerometers at the surface extending 2 meters outward from the source and a second array buried 20 cm directly below the first. Data from this experiment are depicted in Figure 5. Figure 5A shows data taken on two axes of a surface-mounted accelerometer located two meters from the source. These data have been twice integrated in time to represent displacement at the point of measurement. The x-axis is oriented directly away from the source and the z-axis is vertically upward. Hodograms showing the displacement histories for the two arrivals are plotted below this figure. In the hodograms, the vertical displacement (normal to the surface) is plotted versus the horizontal displacement (away from the seismic source); the arrows indicate the direction of time from start to finish in order to designate prograde and retrograde motion clearly. It can be seen from these that the first arrival is associated with a prograde motion consistent with its identity as a leaky wave. The second arrival is retrograde as expected for a Rayleigh wave. Figure 5b depicts the measurement 20 cm below the point represented by 5A. Here the first arrival slightly precedes that which was observed at the surface and is characterized by a linear motion directed toward the source. This is consistent with a P-wave. Motion of the second arrival is prograde at this location, which is consistent with the polarity reversal expected of a Rayleigh wave below the surface. Thus, although the medium is well characterized by the material properties reported in references 8 and 9, the wave field at the surface is more accurately described by the phenomenology reported in reference 10.

4. HARMONIC GENERATION AND NONLINEAR STEEPENING

As mentioned previously, the incident signals used for these experiments were swept-frequency chirps. This makes it possible to separate certain nonlinear effects in the long-time domain using a short-time Fourier transform as a function of measurement times (i.e., a spectrogram). Figure 6 depicts such a spectrogram for the signal received at an accelerometer located 50 cm from the seismic source on dry sand (above the high water mark) at the field test site. The lowest of the positively sloped ridges on the contour plot represents the fundamental component of the drive signal. The ridges with steeper slopes represent each of the higher harmonics generated in the source to sensor path as indicated by the numbers on the plot. Thus, it is a relatively simple matter to distinguish the 200 Hz, 300 Hz, and 400 Hz components generated by nonlinear mechanisms from the same spectral components contained in the original drive signal because these effects are not concurrent on a long timescale. It is clear from the figure that the system is highly nonlinear with more than 8 harmonics distinguishable above the noise floor. The aliasing problem mentioned earlier is also clear in this figure. Although the drive signal contains no energy above 1 kHz, the harmonics of the drive signal higher than the second contain energy above the Nyquist frequency of 4 kHz. Thus, the ridges appear to reflect from the upper frequency bound of the figure. At the times when these aliased signals are coincident with the drive or other harmonics, the two effects cannot be separated in post-processing. In the absence of this aliasing, each of the harmonic components is separated in the time domain and does not, in general, impact the waveforms derived by pulse compression. Both plots in Figure 6 depict the same signal spectrogram. In Figure 6B, the dynamic range has been compressed and converted to a gray scale, which uses only the bottom 20 dB of the 60-dB dynamic range available above the noise floor. From this figure, it is apparent that sub-harmonics of the drive signal are also generated at very low levels in the wave propagation. These features are observable to a lesser extent in data recorded in the laboratory model, but are not evident above the noise floor in the data recorded at the field site during low tide. All of the data show a wealth of higher harmonics at high drive levels.

It is difficult to attribute the generation of the higher harmonics and sub harmonics solely to the nonlinearity of the sand. Source nonlinearity and nonlinearity in the source-to-sand coupling may also play a role in the observed phenomena. Spectral analysis of multiple points along the propagation path shows that, across most of the measurement region ranging from 0.35 m to 5.0 m from the source, there is no enhancement of energy in the overtones. The question remains, however, as to whether or not there is a distinguishable exchange of energy between fundamental frequencies and overtones within the measured region. This is somewhat difficult to address because geometrical spreading reduces the signal with distance, and the higher frequencies are attenuated very quickly in the sand. The absence of an obvious growth of harmonics, therefore, cannot be taken as evidence against the removal of significant energy from the fundamental through harmonic generation. However, an examination of a similar experimental setup from the laboratory reveals evidence to support propagation path nonlinearity as a cause of the harmonics observed in the field tests. Figure 7 shows a comparison between spectra that were observed in the sand and at the source. Although harmonics of the drive signal exist at the source, they have clearly been amplified relative to the fundamental by the first 35 cm of propagation through the sand. Only three overtones are observable in the source motion and six can be seen in the sand. Further evidence in support of this is available from an examination of waveforms from the laboratory model in the time domain. Figure 8 depicts measurements made using a brief time window of a very slow frequency sweep at an instantaneous frequency of 454 Hz. The sweep rate is sufficiently slow that this is equivalent to the results that would be obtained with a CW drive signal at that frequency. A single cycle of the vertical (Z) has been plotted for the source (Figure 8A) and at three measurement locations in Figures 8B, 8C, and 8D. The waveforms in each of these drive signals represent a progressive increase in the level of the current driving the source in 3 dB steps from the smallest measurable signals (1) to the largest (16). Figure 8B shows the motion directly below the source. Here the motion is primarily due to the direct arrival of the compressional wave and is dominantly vertical. With increasing drive levels the waveform distorts in a manner similar to the formation of a shock in a fluid with some directional asymmetry. Figures 8C and 8D depict measurements made at the sand surface 22 cm and 54 cm from the source. Here the shape of the waveform evolves in a manner much less like the classical sawtooth waveform. However, this is somewhat consistent with the numerical predictions of Zabolotskaya for the

vertical displacement component of a nonlinear Rayleigh wave in a homogeneous solid (steel)[13]. It is interesting to note that over the first 50 cm of propagation a significant phase delay occurs in the larger amplitude signals. This is apparent not only in the amplitude peaks, as it would be in a classical Fubini solution for one-dimensional wave propagation, but also in the zero crossings. Their small amplitude would seem to require that these propagate at the linear speed for the medium. The apparent slowing phenomenon was originally attributed to a change in the weighting of the various modes of propagation, however recent data and the work of other researchers [14] suggest that this is due to the hysteretic nature of nonlinearity in soils.

5. SATURATION AND SPALL

There are two obvious limits to the transfer of energy into seismic waves: saturation and spall. Under saturation, marginal level additions to the drive signal are entirely converted into higher harmonics and attenuated so that they make no contribution to the signal level received far from the source where the fundamental component dominates. Thus, an increase in drive signal does not produce a corresponding increase in the amplitude of the propagating elastic wave. Detachment of the source from the sand surface, known as spall, is the solid equivalent of cavitation at the face of an acoustic transducer immersed in a fluid. This occurs when either the biasing force on the shaker contact (the weight of the shaker itself for the data presented here) or the cohesion within the sand below that contact point is inadequate to maintain contact between the source and the sand.

Experimental evidence indicates that each of these mechanisms may limit energy transfer under different circumstances both in the laboratory model and at the field test site. Also, there is some evidence to suggest that the two effects may not be entirely separable in that spalling on a granular scale may be involved in the saturation limit. Spall at the source occurred more readily at the field test site in the measurements performed on the dry sand above the high water mark. It was audible during the tests as a rumble midway through some of the frequency sweeps. Figure 9 depicts a spectrogram containing a spall event measured 51 cm from the shaker source on dry sand; unfortunately, the signals measured by accelerometers closer to the seismic source clipped in the analog electronics during this event. The event is seen midway through the signal and is easily distinguishable from the harmonic generation, which precedes and succeeds it, because of its broadband nature. Both before and after the event, energy is confined to discrete bands around the drive frequency and its overtones, whereas the rupture of the sand distributes energy evenly over the entire bandwidth of the measurement system and probably beyond this as well. Although the force applied to the contact surface was constant through the drive signal, the contact has obviously been restored after the spall event. This is probably because the sand surrounding the contact was fluidized by the spall event, and the settling of the shaker into the surface improved the contact sufficiently to end the event.

All of the field measurements were performed with transient signals using a sparse set of empirically determined drive levels; unfortunately, the point at which individual spectral components of the drive signal went into saturation could not be determined from this limited data set. The experiment was therefore repeated in the laboratory model using a pure tone drive at 396 Hz (near the middle of the band of interest). The results of this experiment are plotted in Figure 10. Here the measured levels of the fundamental component and the first two harmonics have been plotted for the acceleration measured in the sand at 4 different ranges against that measured at the source. All of the curves depict a nominally linear amplitude ratio for source accelerations up to about 1 g. Beyond this, the received signals begin to saturate. Interestingly, the signals measured at 61 cm and 122 cm from the source enter a phase where incremental additions to source level result in an actual decrease in measured acceleration of the sand. This may be due to an interference, which occurs when portions of the source contact have fluidized while others have not. It is also possible that the combined effects of dispersion, changes to the relative weighting of propagation modes, and regeneration of the fundamental frequency by mixing of overtones produces a destructive interference.

6. NONLINEAR DISPERSION

Dispersion can be observed in measured surface waveforms in most of the data from both the laboratory model and the field site. It is apparent in the change in pulse shape as a function of location shown in Figures 3 and 4. The nature of this dispersion has significant implications for the post-processing of experimental data. Linear dispersion of Rayleigh waves, which can occur as a consequence of the vertical gradients in material properties, is fully accounted for in the pulse compression routine that generated the waveforms depicted in Figures 3 and 4. Nonlinear dispersion, however, is not intrinsically accounted for, since sum and difference frequencies occur at times that are dependent on pulse shape and therefore shift in time during the compression, which presumes that they are causally linked to the identical spectral components of the compressed drive signal. This produces artifacts with apparent delays that do not correspond to any of the physical processes and often precede the generation of the incident signal. The differences between linear and nonlinear dispersion are illustrated by the laboratory results shown in Figure 11. Here, the acceleration was measured at four separate locations on the sand surface using a differentiated Gaussian pulse with a center frequency of 450 Hz as the original drive signal rather than reconstructing the pulse response in post-processing. The figure shows raw data, although 1000 pulses have been averaged together to build up the signal-to-noise ratios for each measurement. The horizontal separation in Figure 11 indicates the four different measurement locations in the model at 30.5 cm, 61 cm, 122 cm, and 244 cm along a line away from the source. The magnitude of the offset is arbitrary. Propagation delays of 3 ms, 6 ms, 16 ms, and 31 ms have been subtracted before the waveforms were stacked so that all the data could be displayed in a single graph. Each vertical separation between traces indicates an increase of 3 dB in drive signal amplitude. The signals have all been normalized by their own peak levels in order to emphasize changes in the delay and the shape of the pulse over amplitude differences. Actual amplitude differences of approximately three orders of magnitude are suppressed in this way for the data depicted in the figure.

The apparent inversion of the signal between the first and second measurement points at very low drive levels is an indication of linear dispersion. Viewed as a function of position, the peaks and troughs of the signal can be seen to propagate through the pulse envelope as this envelope propagates across the sand surface. The obvious change in pulse shape and the delays associated with the pulse arrival at high drive levels are the effect of nonlinear dispersion. The troughs of the original pulse can be seen to form two downward acceleration impulses 30 cm from the source, similar to those depicted in Figure 7 for a continuous drive. These impulses separate in time as drive level is increased, much like the broadening of shock waves observed in air [15]. At greater distances there is, however, a preference toward not only the low frequency components of the original pulse, but also the energy that arrives late in time. This is particularly apparent in the data taken at 61 cm where the arrival of the pulse is visibly delayed with increasing drive. This inverse relationship between the drive level and group velocity can be explained by hysteresis in the medium or by a loss mechanism which preferentially attacks the leading edge of a pulse as it broadens in time similar to an N-wave. The fact that a similar effect is observed in the phase velocity of CW signals supports the first of these explanations. In particulate media it has been observed that bulk shear waves slow down at high drive levels rather than steepening as P-waves do [14]. Since the pulse of interest here, and the dominant source of surface motion depicted in Figure 7, are surface waves that are primarily shear-like, this explanation appears to be consistent with the available literature. Interestingly, this slowing phenomenon can be reproduced by linear pulse compression begun with a variety of incident time waveforms including the frequency swept chirp discussed earlier, a pseudo-random noise signal, and a spectrally discrete continuous waveform that spans the frequency range of interest. Because of the arrival time differences associated with signal harmonics, the nonlinear distortion of the pulse shape cannot be accurately reproduced in this way.

7. CONCLUSIONS

Measurements have been conducted at a field test site and in a laboratory model that qualify the role played by system nonlinearity in limiting the potential range and signal level that can be exploited by a seismic mine detection system. Propagation of elastic waves in the linear regime at both of these sites is reasonably well

understood and in good agreement with published theory and observations. Nonlinearity in both the source coupling and the propagation path were observed at both sites and demonstrated to be possible limiting factors for a seismic landmine detection system. Observed steepening and nonlinear dispersion pose potential problems for the post-processing of data in that they undermine pulse compression schemes that can be used to improve the signal to noise ratio in the linear regime. The dependence of propagation speed on drive level appears to be transparent to this sort of processing, but may pose problems in the wavenumber analysis used in the imaging algorithms thereby limiting usable drive signal levels. Work is currently underway to understand and quantify all of these effects and their potential impact on system operations.

8. ACKNOWLEDGEMENTS

This work is supported by the Office of Naval Research under contact number N00014-99-1-0995 and contract number N00014-01-1-0743. The authors would like to thank Dr. Thomas G. Muir for his assistance in the conduct of the field experiments and interpretation of the data. Portions of this paper were published as part of a conference proceedings [16].

9. REFERENCES

1. Patel, D.L., "Handbook of Land Mines and Military Explosives for Countermine Exploitation," *US Army Belvoir RD&E Center Technical Report No. 2495*, March 1992.
2. Scott W.R., Jr., Larson, G.D., and Martin, J.S., "Simultaneous Use of Elastic and Electromagnetic Waves for the Detection of Buried Land Mines," *Proceedings of the SPIE: 2000 Annual International Symposium on Aerospace/Defense Sensing, Simulation, and Controls*, Orlando, FL, Vol. 4038, April 2000.
3. Scott, W.R., Jr., Martin, J.S., and Larson, G.D., "Experimental Model for a Seismic Landmine Detection System," *IEEE Transactions on Geoscience and Remote Sensing*, Vol. 39, pp. 1155-1164, July 2001.
4. "Feasibility of Acoustic Landmine Detection: Final Technical Report," *BBN Technical Report No. 7677*, May 1992.
5. Behboodian, A., Scott, W.R., Jr., and McClellan, J.H., "Signal Processing of Elastic Surface Waves for Localizing Buried Land Mines," *Proceedings of the 33rd Assilomar Conference on Signals, Systems, and Computers*, Assilomar, CA, October 1999.
6. Sabatier, J.M., Bass E.H., Bolen, L.N., and Attenborough, K., "Acoustically Induced Seismic Waves," *Journal of the Acoustical Society of America*, Vol. 80, no. 2, pp. 646-9, August 1986.
7. Westebbe, M., Bohme, J.F., Krummel, H., and Matthews, M.B., "Model fitting and testing in near surface seismics using maximum likelihood in frequency domain," *Conference Record of thirty-second Asilomar Conference on Signals, Systems and Computers*, Vol. 2, pp.1311-15, November 1998.
8. Bachrach, R., and Nur, A., "High-Resolution Shallow-Seismic Experiments in Sand, Part I: Water Table, Fluid Flow, and Saturation," *Geophysics*, Vol. 63, No. 4, pp. 1225-1233, July 1998.
9. Bachrach, R., Dvorkin, J., and Nur, A., "High-Resolution Shallow-Seismic Experiments in Sand, Part II: Velocities in Shallow Unconsolidated Sand," *Geophysics*, Vol. 63, No. 4, pp. 1234-1240, July 1998.
10. Smith, P., Wilson P.S., Bacon F.W., Manning, J.F., Behrens, J.A., and Muir T.G, "Measurement and Localization of Interface Wave Reflections from a Buried Target," *Journal of the Acoustical Society of America*, Vol. 103, no. 5, pp. 2333-43, May 1998.
11. Lay, T., and Wallace, T.C., "*Modern Global Seismology*," NY: Academic Press, 1995, pp. 252-63.

12. Schröder C. T., and Scott W. R. Jr., "On the Complex Conjugate Roots of the Rayleigh Equation: The Leaky Surface Wave," *Journal of the Acoustical Society of America*, Vol. 110, no. 6, pp. 2867-77, December 2001.

13. Zabolotskaya, E.A., "Nonlinear Propagation of Plane and Circular Rayleigh Waves in Isotropic Solids," *Journal of the Acoustical Society of America*, Vol. 91, no. 5, pp. 2569-75, May 1992.

14. Santamarina, C. J., Klein, K.A., and Fam, M. A., "*Soils and Waves*," NY, John Wiley and Sons, 2001, pp. 103-115 and pp. 246-7

15. Beyer, R.T., "*Nonlinear Acoustics*." NY: Acoustical Society of America Press, 1997, pp. 91-109 and pp. 189-202.

16. Larson, G.D., Martin, J.S., Scott, W.R., Jr., and McCall, G.S., II, "Environmental Factors that Impact the Performance of a Seismic Land Mine Detection System," *Proceedings of the SPIE: 2001 Annual International Symposium on Aerospace/Defense Sensing, Simulation, and Controls*, Orlando, FL, Vol. 4394, pp. 563-574, April 2001.

10. LIST OF FIGURES

Figure 1: Configuration of Seismic Landmine Detection System.

Figure 2: Experimental Models: (A) the Laboratory Model and (B) the Field Test Site.

Figure 3: Propagation of a Seismic Pulse in (A) the Laboratory Model and (B) at the Field Test Site.

Figure 4: Comparison of Wave-Front Transects: (A) Propagation Parallel to the Beach and (B) Shoreward Propagation.

Figure 5: Displacements Measured at Two Locations in the Laboratory Model: (A) At the Surface 2 m from the Source and (B) 20 cm Below the Surface 2 m from the Source.

Figure 6: Spectrogram of Acceleration Signal Measured 50 cm from the Seismic Source at the Field Site on Dry Sand, Depicted (A) on a 60 dB Scale and (B) on a 20 dB Scale at the Bottom of the Dynamic Range Measured.

Figure 7: Spectrograms of Measured Acceleration on a 60 dB Dynamic Range Measured (A) at the Source and (B) in the Sand 30.5 cm from the Source in the Laboratory Experimental Model.

Figure 8: Distortion of a 454 Hz Signal at Various Locations: (A) Source, (B) 20 cm Below the Source, (C) on the Surface 22 cm from the Source, and (D) on the Surface 54 cm from the Source.

Figure 9: Spectrogram of a Spall Event Measured at the Field Site 46 cm from the Source on Dry Sand.

Figure 10: Measured Levels of (A) 396 Hz Fundamental, (B) First Harmonic, and (C) Second Harmonic in Sand vs. Source Motion.

Figure 11: Surface Vertical Acceleration Pulse Shapes as a Function of Drive Level and Range.

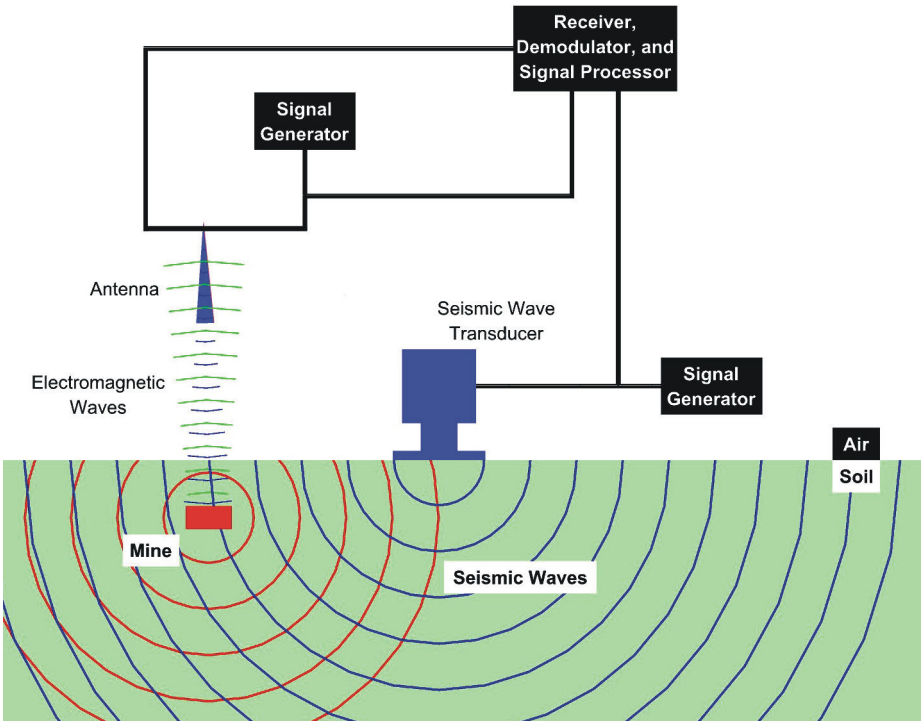

Figure 1: Configuration of Seismic Landmine Detection System.

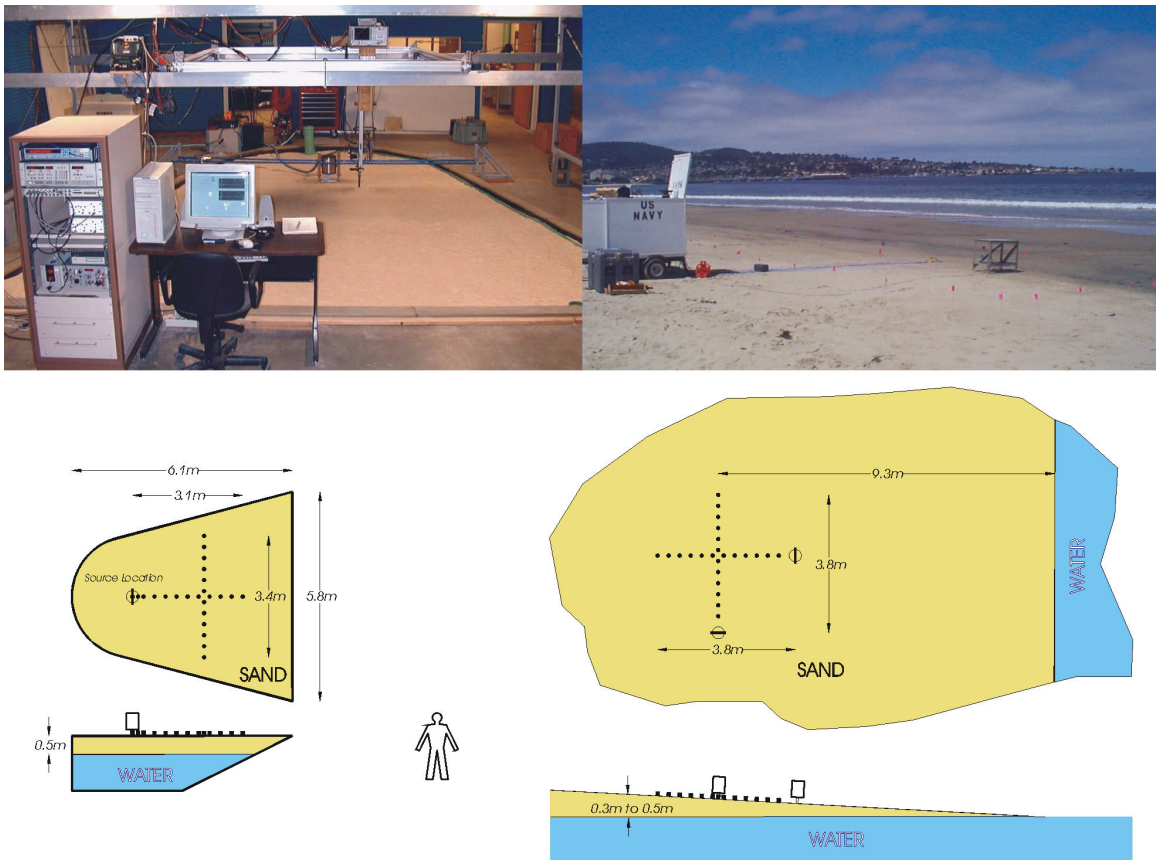

Figure 2: Experimental Models: (A) the Laboratory Model and (B) the Field Test Site.

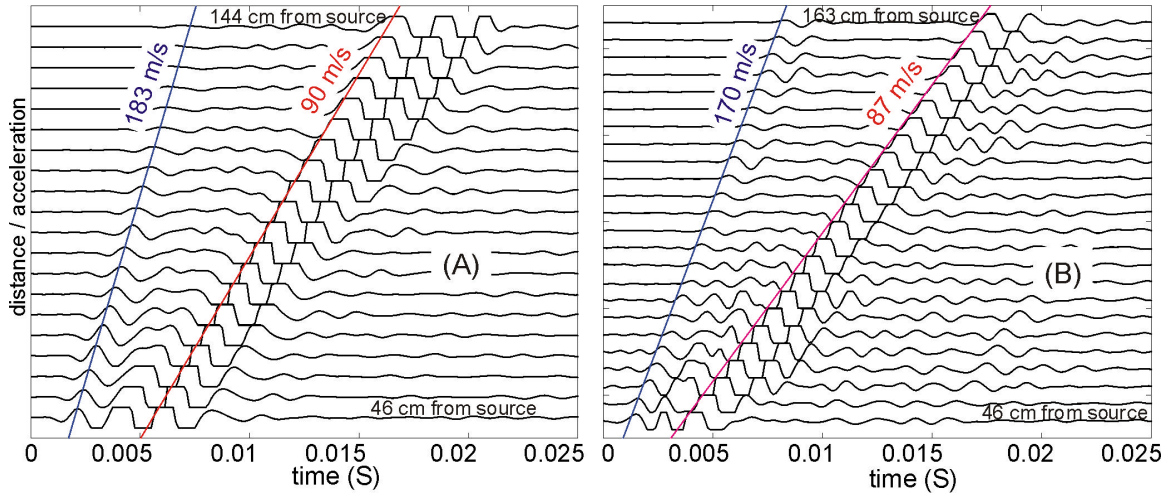

Figure 3: Propagation of a Seismic Pulse in (A) the Laboratory Model and (B) at the Field Test Site.

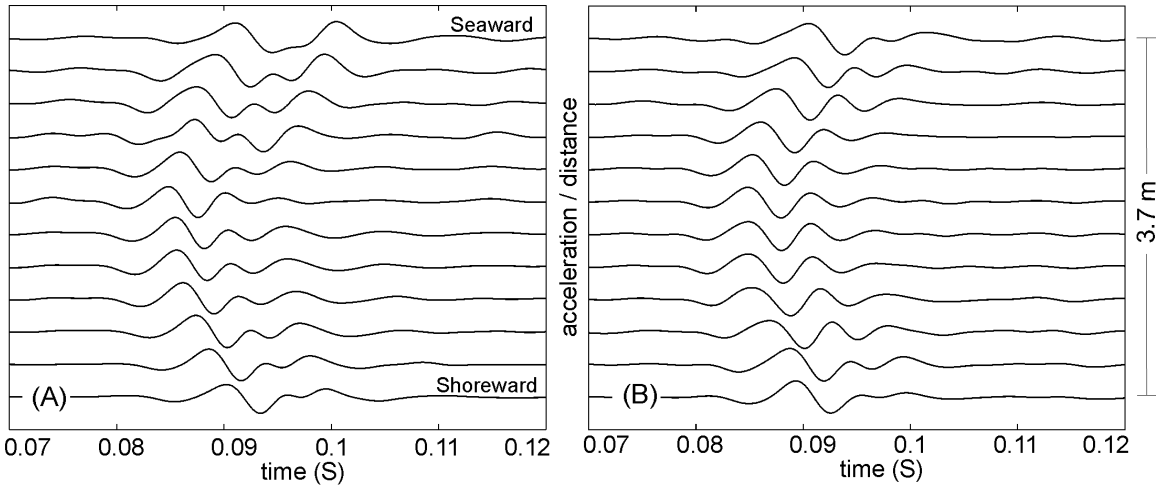

Figure 4: Comparison of Wave-Front Transects: (A) Propagation Parallel to the Beach and (B) Shoreward Propagation.

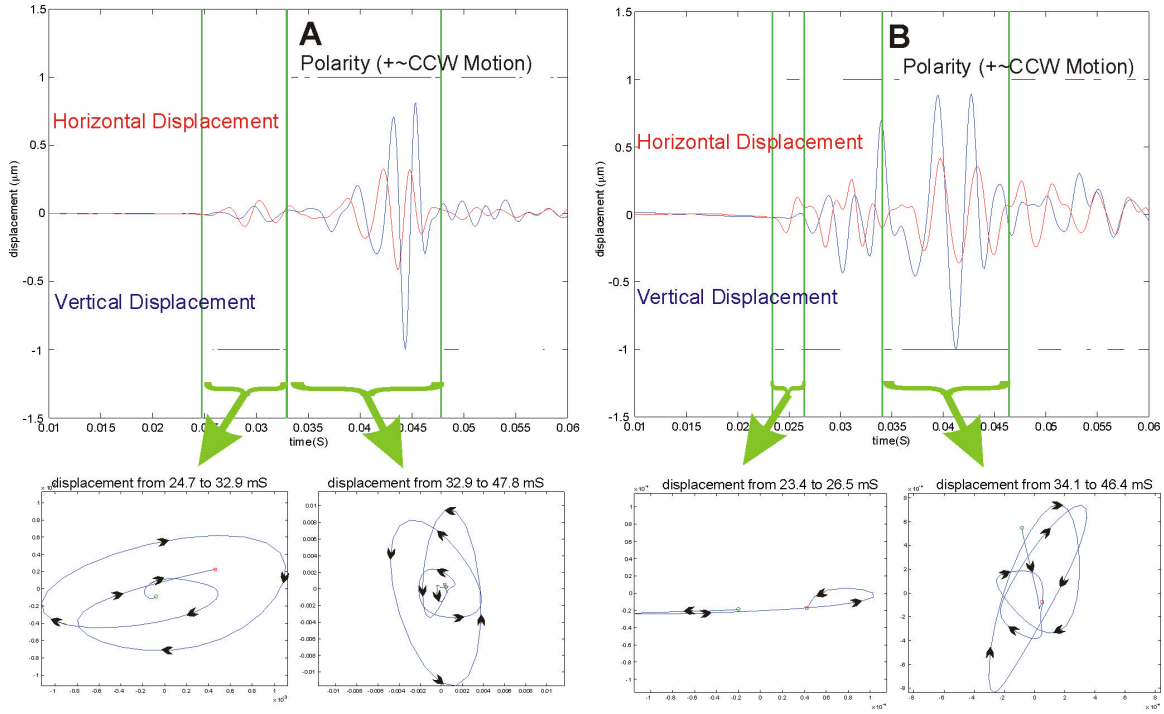

Figure 5: Displacements Measured at Two Locations in the Laboratory Model: (A) At the Surface 2 m from the Source and (B) 20 cm Below the Surface 2 m from the Source.

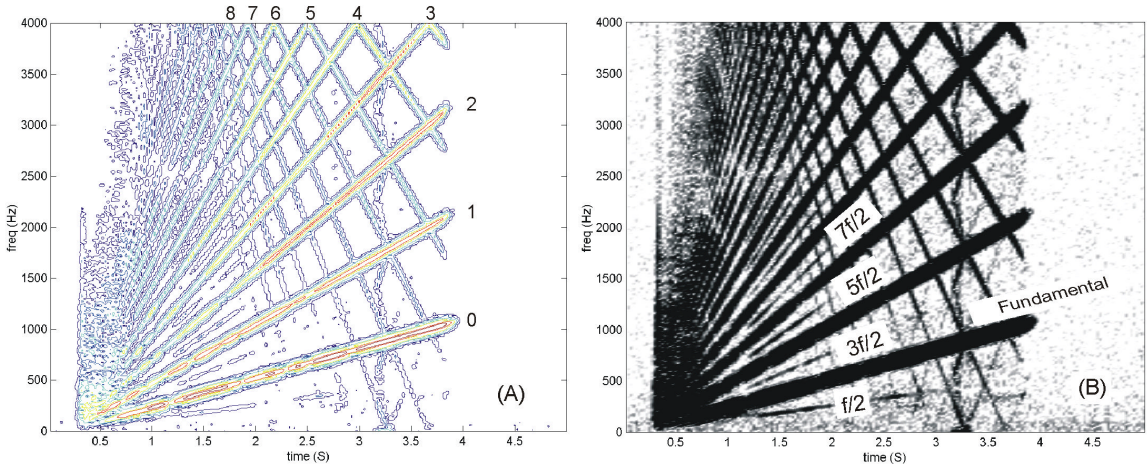

Figure 6: Spectrogram of Acceleration Signal Measured 50 cm from the Seismic Source at the Field Site on Dry Sand, Depicted (A) on a 60 dB Scale and (B) on a 20 dB Scale at the Bottom of the Dynamic Range Measured.

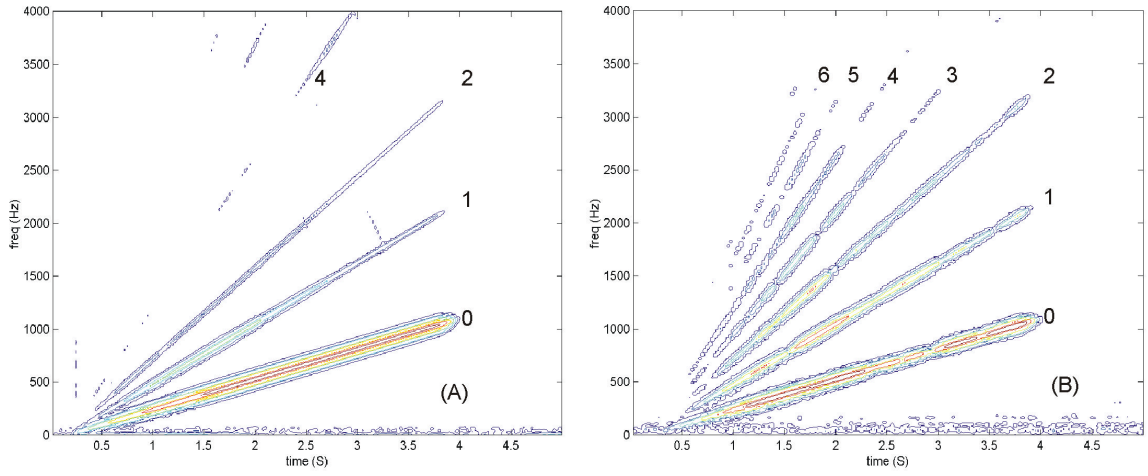

Figure 7: Spectrograms of Measured Acceleration on a 60 dB Dynamic Range Measured (A) at the Source and (B) in the Sand 30.5 cm from the Source in the Laboratory Experimental Model.

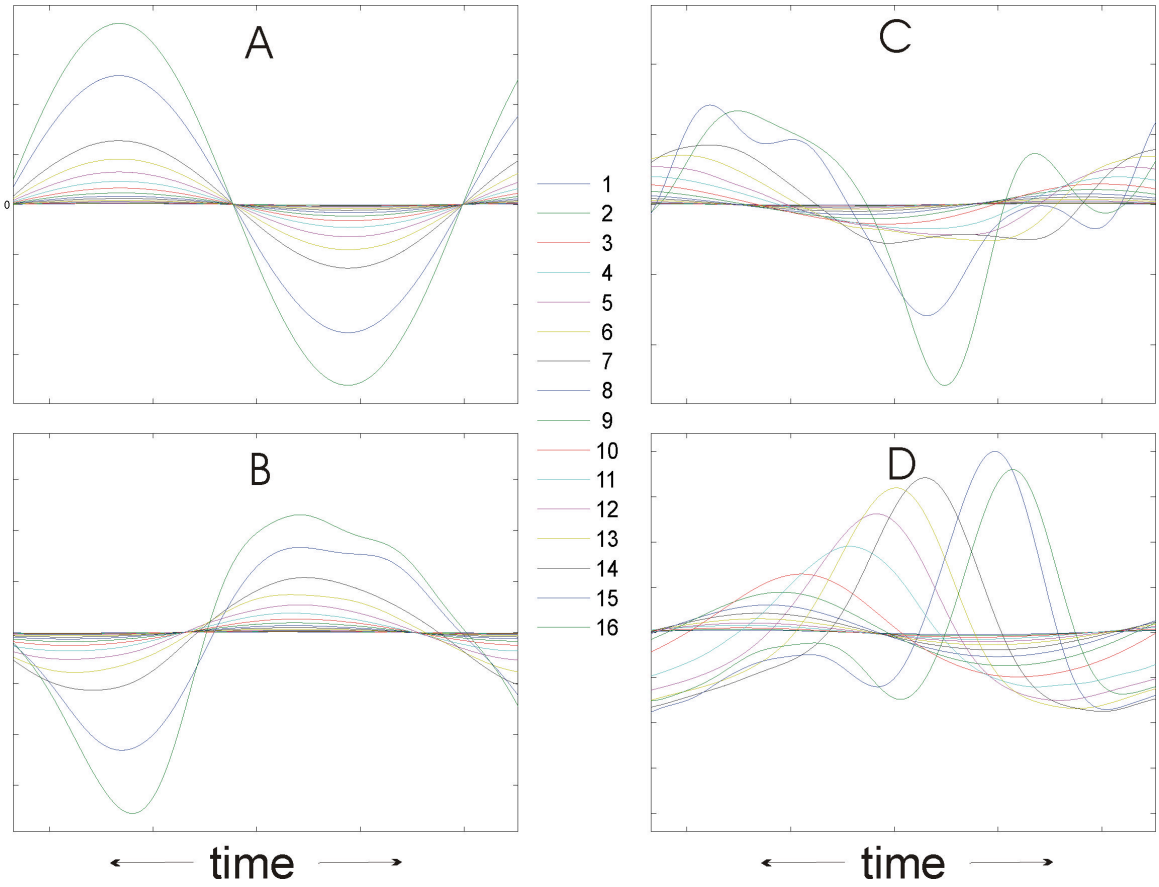

Figure 8: Distortion of a 454 Hz Signal at Various Locations: (A) Source, (B) 20 cm Below the Source, (C) on the Surface 22 cm from the Source, and (D) on the Surface 54 cm from the Source.

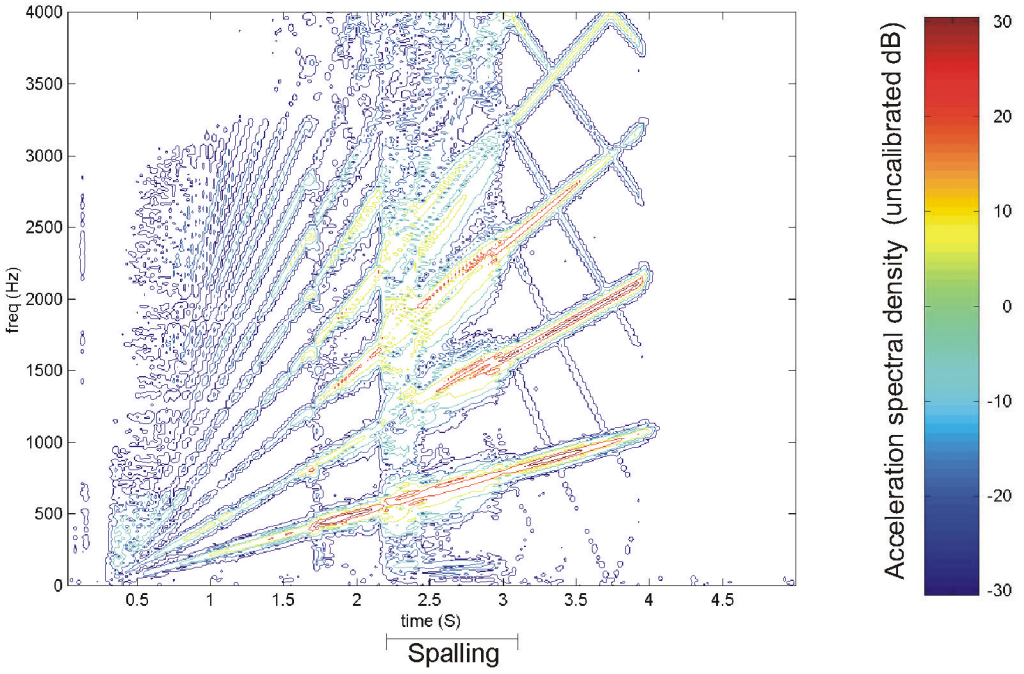

Figure 9: Spectrogram of a Spall Event Measured at the Field Site 46 cm from the Source on Dry Sand.

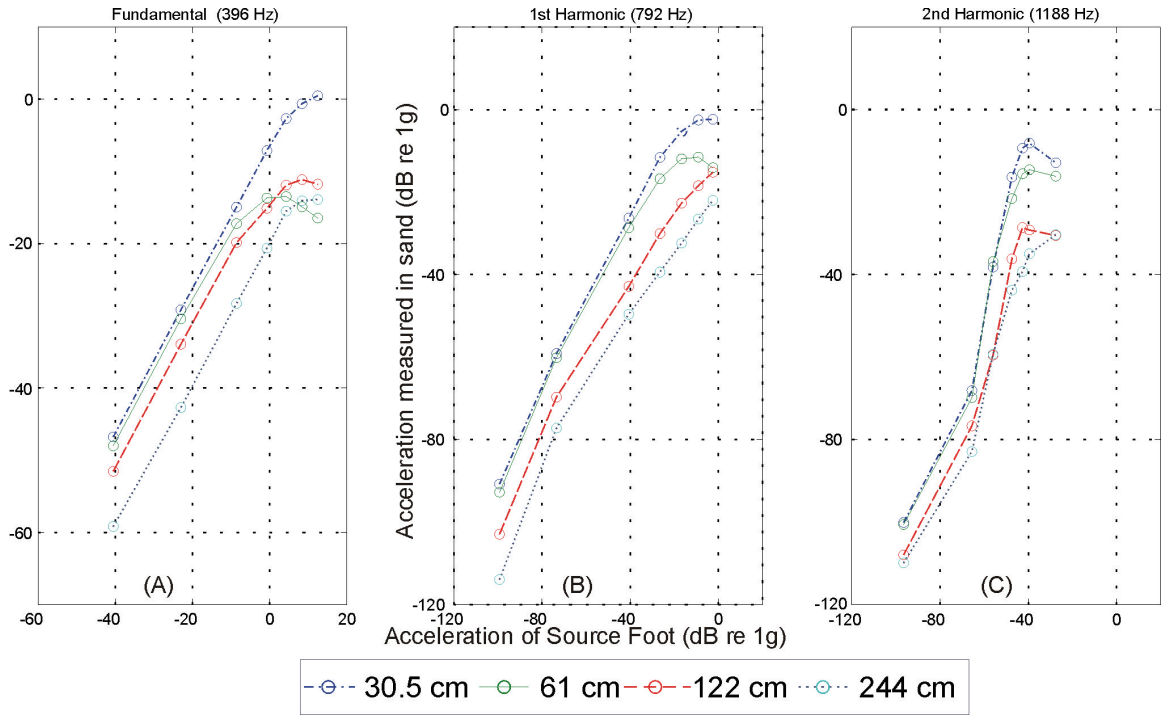

Figure 10: Measured Levels of (A) 396 Hz Fundamental, (B) First Harmonic, and (C) Second Harmonic in Sand vs. Source Motion.

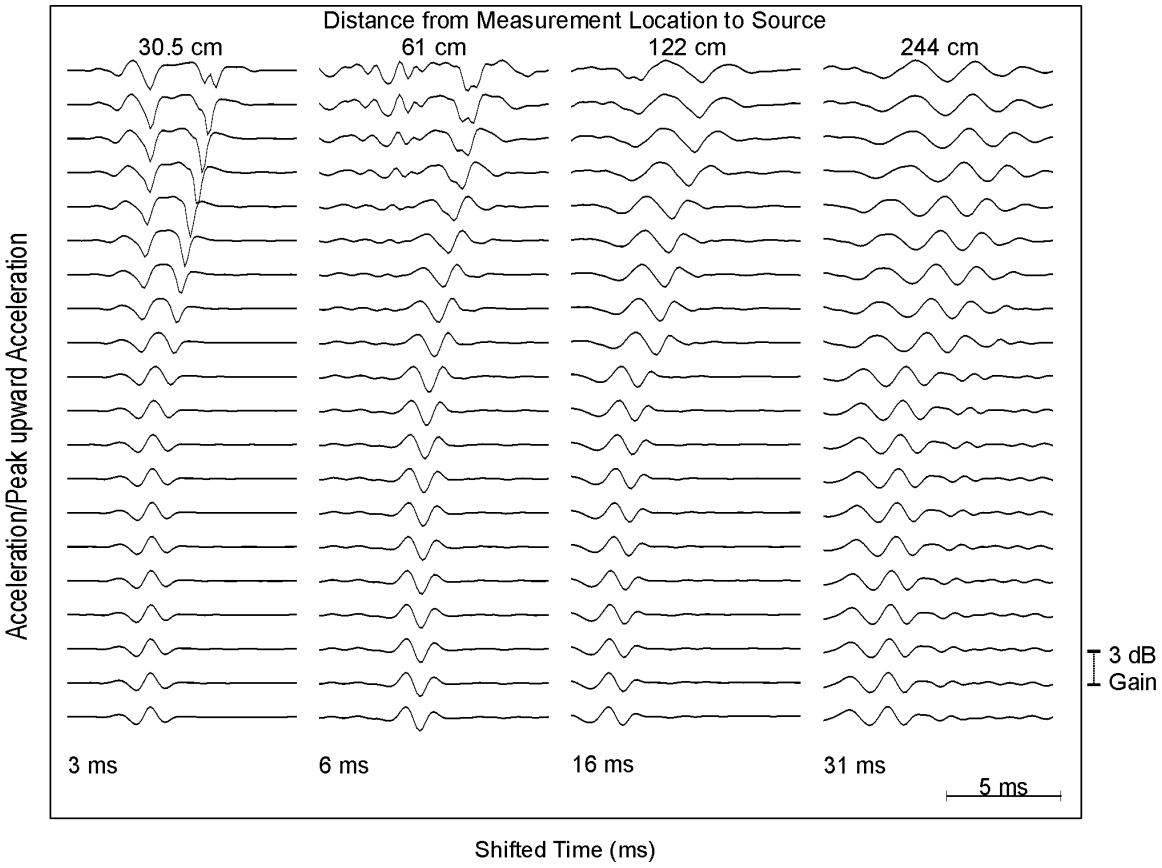

Figure 11: Surface Vertical Acceleration Pulse Shapes as a Function of Drive Level and Range.